BIOCHEMISTRY

 Volume 43, Number 28 July 20, 2004

Current Topics

Following Ligand Binding and Ligand Reactions in Proteins via Raman Crystallography†

Paul R. Carey* and Jian Dong

Department of Biochemistry, Case Western Reserve University, Cleveland, Ohio 44106

Received April 28, 2004; Revised Manuscript Received June 8, 2004

ABSTRACT: Raman crystallography permits the monitoring of chemical events in single-protein crystals in real time. Using a Raman microscope, it is possible to obtain protein Raman spectroscopic data of unprecedented quality and stability. The latter features allow us to obtain the Raman spectrum for small molecules soaking into crystals under normal (nonresonance) Raman conditions. Thus, via an approach utilizing Raman difference spectroscopy, we can quantitate the amount of ligand in the crystal, determine the chemistry of inhibitor−protein interactions, and follow chemical reactions in the active site on the time scale of minutes. While providing unique chemical insights, these data also provide an invaluable guide for determining the conditions for flash-freezing crystals for X-ray crystallographic analysis. In addition, the Raman difference spectra often contain contributions from protein modes due to protein conformational changes occurring upon ligand binding. These features allow us to probe events ranging from small cooperative conformational changes to massive and unexpected secondary structure changes in the crystal. An experimental advantage of Raman crystallography is that the data can be collected from crystals *in situ*, in sitting or hanging drops, under the conditions used to grow the crystals.

What is Raman Crystallography?

The Raman, or resonance Raman, spectrum of a substrate bound to an enzyme's active site can be the source of unique mechanistic insights (*1*, *2*). However, in the absence of a chromophoric substrate to provide an intensity-enhanced spectrum, the Raman spectrum of the substrate is often obscured by the thousands of vibrational modes from the protein. Callender, Deng, and co-workers showed that this limitation can be overcome in part by using a difference spectroscopic approach (*3*). Via subtraction of the Raman spectrum of the enzyme from that of the enzyme−substrate complex, the Raman spectrum of the bound substrate is revealed, along with some contributions from protein modes if substrate binding brings about protein conformational change. Since the difference approach involves detecting the tiny contribution of the substrate to the composite enzyme−substrate spectrum, the parent spectra must have a high signal-to-noise ratio and be very stable. In practice, this becomes a severe limitation to general applicability. However, we have shown recently that single crystals are an ideal platform for the Raman difference approach. Using a Raman microscope, very high signal-to-noise ratio data sets are obtained that have very low and stable underlying spectral backgrounds. Thus, it has become almost routine in our laboratory to "follow" ligands soaking into crystals, via the Raman difference spectrum, occurring at room temperature on the time scale of tens of seconds. While the Raman data themselves provide unique insight into ligand binding, at the same time they become a powerful aid to X-ray crystallo-

† Supported by National Institutes of Health Grants GM 54072 and DK 53053.

* To whom correspondence should be addressed. E-mail: prc5@cwru.edu. Phone: (216) 368-0031. Fax: (216) 368-3419.

10.1021/bi049138a CCC: $27.50
Published on Web 06/24/2004

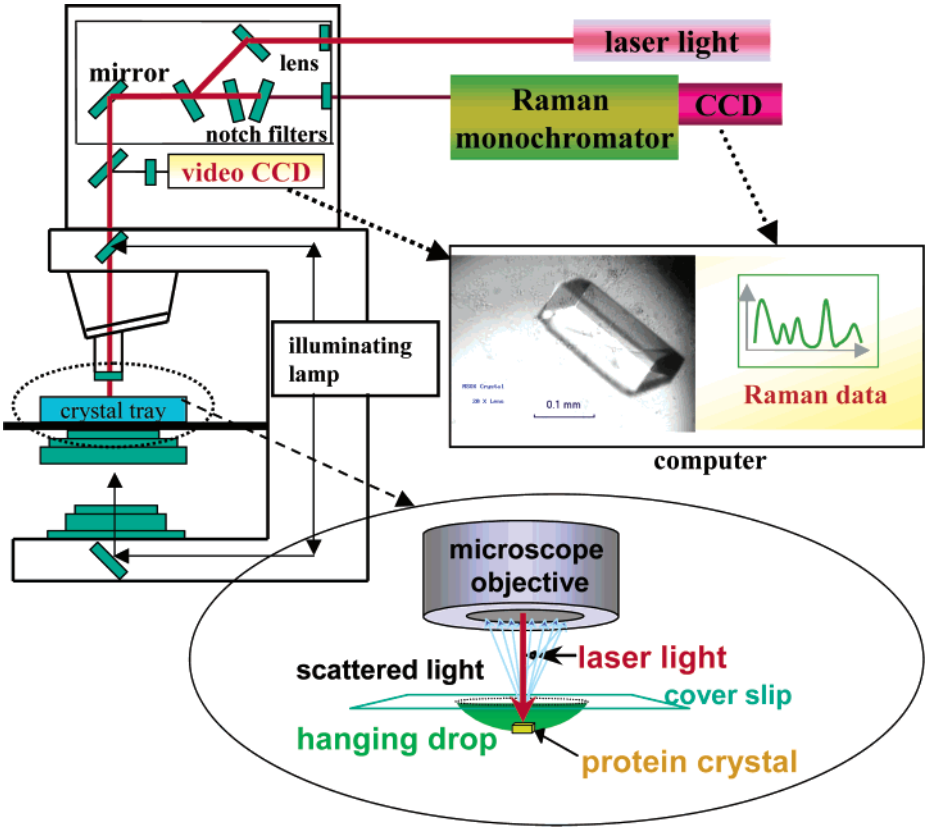

FIGURE 1: Raman microscope coupled to a krypton laser and a spectrometer. Both video images and spectral data can be displayed in real time on the computer screen. Also shown is a magnified view of a protein crystal in a hanging drop under the microscope objective.

graphic experiments. Since the Raman data provide quantitative estimates of the species in active sites in the crystal, they define the conditions for soaking and flash-freezing and for subsequently determining the structures of well-defined enzyme−inhibitor or enzyme−substrate complexes.

Historical Background

While the use of a Raman microscope in obtaining Raman difference data from crystals is a recent innovation, spectroscopists realized soon after the introduction of lasers that single-crystal Raman spectroscopy was feasible. In the early 1970s, Yu and co-workers compared the crystal and solution Raman spectra for proteins such as α-lactalbumin, insulin, and glucagon (*4* and references therein). In these heroic studies, protein single crystals were mounted in a cuvette or glass vial, positioned "by eye" at the focal point of the fore-optics, that is, directly at the front of a standard Raman instrument. The work provided some of the earliest evidence that the main chain structures of proteins in crystals are similar to those in solution and crystallization has no detectable effect on the backbone conformation. Small differences observed between crystal and solution Raman data were interpreted in terms of changes in amino acid side chain conformations. In a similar way, resonance Raman spectroscopy was used to study the heme moieties in cytochrome P450 and myoglobin protein crystals (*5*, *6*). The active site heme structures were found to be identical for the crystal and solution phase. The 1980s and 1990s heralded new technologies permitting the development of Raman microscopy, where an optical microscope is coupled to a Raman spectrometer to collect Raman signals from sample regions as small as a few micrometers across. This found applications in cell biology (*7*, *8*) as well as in heme protein crystal studies. Most of the latter involved the peroxidase family (*9*), and since they were carried out under resonance Raman conditions, very low laser power had to be used to minimize photodegradation induced by the laser beam. Only a handful of nonresonance Raman microscopic studies of protein crystals were reported in the 1980s and 1990s. G. J. Thomas's group found small differences in the Raman intensities of side chains of subunits in the empty capsid of bean pod mottle virus (*10*) and in the *Ff* gene V protein (*11*) in crystalline and solution states. These differences were interpreted as the result of changes in a small number of side chain environments between crystal and solution, finding a parallel to Yu's early work. In a study of crystalline DNA−protein complexes, Peticolas and co-workers (*12*) were able to detect major changes in the conformation of oligonucleotide d(TCGCGAATTCGCG) binding to the restriction endonuclease *Eco*RI. Importantly, there were two technical advances in the 1990s: the introduction of red light sensitive charge-coupled photon detectors and holography-based notch filters that blocked unwanted elastically scattered photons. Together, these innovations greatly increased the sensitivity of Raman microscopes in the red (600−800 nm) region of the spectrum. This was a critical breakthrough because the Raman microscope could now be operated using laser excitation in the red part of the spectrum, providing protein spectra free from the weak luminescence background that often accompanies excitation in the blue/green (near 500 nm).

The Experiment

A schematic of our Raman microscope is shown in Figure 1. Crystals are usually grown in, or transferred to, hanging drops in a 24-well tray of the kind used by X-ray crystallographers. The tray is placed on the microscope stage, and the crystal in each drop can be viewed via a long focal length objective and a video charge-coupled device (CCD)[1] camera for optical imaging. A laser beam is introduced on the microscope's optical axis using a fiber optic, and the beam focused on the crystal can be viewed on the computer monitor. This provides the degree of experimental control needed since the crystals and focal spot are usually too small (on the scale of tens of micrometers) to be viewed by the naked eye. In the next step, the standard illuminating source is blocked and the backscattered light from the focal spot goes back through the microscope and, via optical filters and a second fiber optic, is fed into a Raman spectrograph. The Raman spectral image at the CCD photon detector then appears on the computer monitor providing the Raman spectrum associated with the focal spot on the crystal. The microscope is operated in the nonconfocal mode to maximize light throughput, and the focal volume is typically 20 μm in diameter and 50 μm in depth that determines a minimal crystal dimension of 30 μm for optimal spectral quality. For most systems, it takes ~100 s to collect a complete data set, using 100 mW of 647.1 nm Kr^+ laser excitation at the sample. When Raman difference spectroscopy is undertaken, care must be exercised to perturb the crystal as little as possible when introducing the ligand into the liquid surrounding the crystal. Moreover, it is important to bear in mind that the intensity of Raman scattering may be dependent on the relative orientations of the crystal axes and the laser beam, a factor that can be used to facilitate the Raman difference method (*13*), but which can also lead to uncontrolled changes in Raman intensity, if not taken into account (*14*).

There are two main reasons why the Raman microscope is so effective and can obtain Raman difference data from complexes that do not yield results in solution. The first is concentration; proteins in crystals are typically at 10−60 mM, which is a range more than 1 order of magnitude higher than maximum solution concentrations. The second is that the microscope, coupled with a red or deep-red excitation source, yields Raman spectra with very low spectral backgrounds that are, moreover, stable (the background does not fluctuate slowly with time). These conditions give rise to sensitive and reproducible Raman difference experiments.

Soaking in, Soaking out. Quantitating Ligand Binding in the Crystal

The Raman difference spectra can be used to follow the introduction of ligands into the crystals by "soaking in". Ligand is added to the mother liquor surrounding an apocrystal to give a final concentration in the 5−15 mM range. By recording sequential Raman difference spectra from the crystal, we see that features from the ligand increase in intensity with time until all the enzyme molecules have a

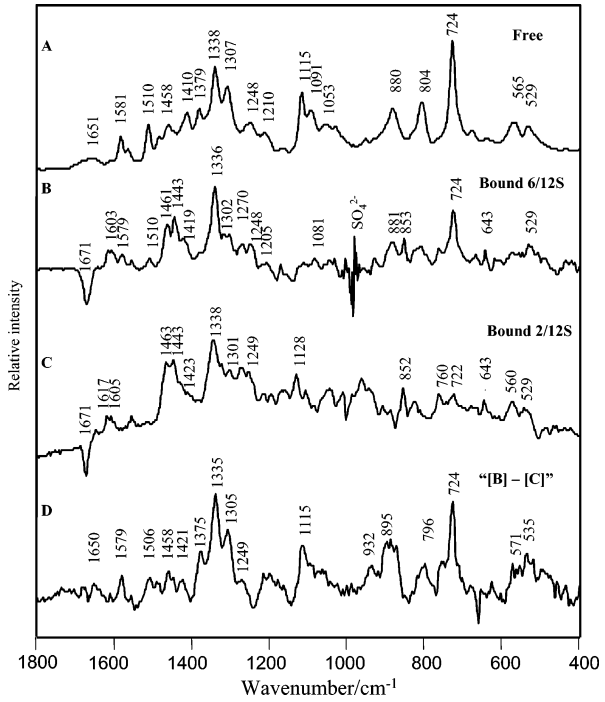

FIGURE 2: Raman difference spectra of methylmalonyl-CoA: (A) [3.5 mM MM-CoA in water] minus [water], (B) [MM-CoA bound to a single crystal of 12S, six molecules of substrate per hexamer] − [apocrystal], (C) [MM-CoA bound to a single crystal of 12S, two molecules of substrate per hexamer] − [apocrystal], and (D) MM-CoA bound to a single crystal of 12S, obtained by subtracting [2MM-CoA-12S] from [6MM-CoA-12S]. These spectra were generated from the same crystal by a soaking-out experiment. Note the derivative feature near 980 cm^{-1} in panel B is due to the presence of sulfate anions.

ligand in their active sites. As an example, consider the binding of substrate to the 12S subunit of the enzyme transcarboxylase (TC) (*15*). TC is a multisubunit enzyme that catalyzes the overall transfer of carboxylate from methylmalonyl-CoA (MM-CoA) to pyruvate to form oxaloacetate and propionyl-CoA. In the first half-reaction, the 12S subunit transfers a carboxylate group from MM-CoA to a biotin group on transcarboxylase's 1.3S subunit (eq 1)

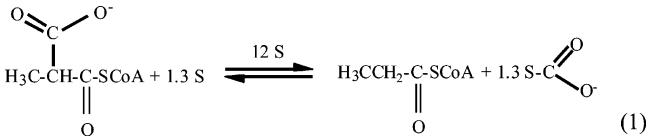

(1)

In solution, 12S functions as a hexamer with a total molecular mass of 336 000 Da, and single crystals of the protein retain the hexameric motif (*16*). MM-CoA can be soaked into the crystal, and in the absence of 1.3S-biotin, no reaction occurs. In the Raman spectrum of MM-CoA in Figure 2A, the most intense modes are due to the adenine moiety on CoA since this is a strong Raman scatterer. The adenine feature at 724 cm^{-1} can be used to follow the time course of soaking in (*17*). In a 5 mM bath of ligand, the intensity of the 724 cm^{-1} band increases as MM-CoA penetrates the 12S crystal and reaches a saturation level in ~1 h. Unbound ligand within the crystal is essentially undetected since it is present at less than 2 mM, a concentration that gives only very weak signals under the Raman microscope. Thus, the intensity of the 724 cm^{-1} peak is directly proportional to the concentration of MM-CoA bound

[1] Abbreviations: TC, transcarboxylase; MM-CoA, methylmalonyl-coenzyme A; UK, urokinase; PHBH, *p*-hydroxybenzoate hydroxylase; *p*-OHB, *p*-hydroxybenzoic acid; 2,4-di-OHB, 2,4-dihydroxybenzoic acid; CCD, charge-coupled device.

Scheme 1. Structures and Inhibition Constants of Urokinase Inhibitors

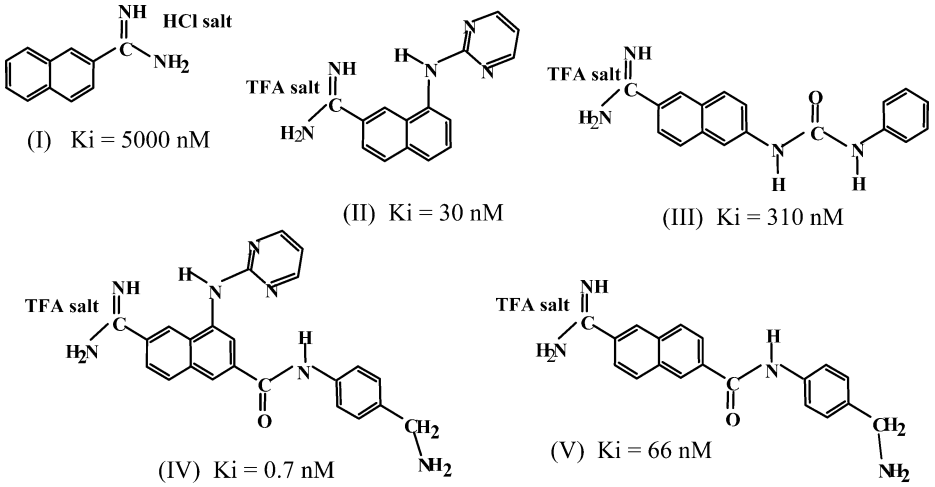

to active sites in the crystal. Using a standard plot of intensity versus concentration for free MM-CoA in solution, the intensity of the 724 cm^{-1} crystal feature yields 11.5 mM for MM-CoA in the crystal. (This approach is only valid for crystal complexes that do not show a strong dependence of Raman intensity on crystal orientation, which is the case here.) The X-ray crystallographic data show that the concentration of the 12S hexamer in the crystal is 2 mM, i.e., 12 mM in monomer. Thus, after soaking had been carried out for 1 h, a stoichiometric 1:1 complex has formed between MM-CoA and each monomer.

Via replacement of the mother liquor containing MM-CoA with substrate-free mother liquor or 60% ammonium sulfate solution, soaking out occurs with the MM-CoA being released and the 724 cm^{-1} band becomes undetectable after 30−60 min. These findings were highly useful in efforts to determine the three-dimensional structure of 12S complexes. Initially, 12S was cocrystallized with MM-CoA, but in the resultant structure, although the CoA could be seen, electron density from the MM group was absent. In the several weeks that were required for the crystallization process, the MM group was removed from the CoA by a slow hydrolysis step. However, in light of the Raman results, CoA was soaked out and fresh MM-CoA soaked in for 1 h. The crystals were flash-frozen, and now electron density could be observed for the MM moiety in the active site. Consonant with the Raman difference data, there are six MM-CoAs bound per 12S hexamer (*16*).

MM-CoA is a fairly large molecule and takes up to 1 h to diffuse fully into a 12S crystal. In other systems, smaller ligands can diffuse in more rapidly. For example, β-lactams diffuse fully into β-lactamase enzyme crystals in ~1 min (*18*). Of course, solvent channel size and active site accessibility are other factors affecting soak-in times.

Drug Compound Screening

If drug targets form crystals that are amenable to soak-in, soak-out experiments, Raman crystallography can be used to screen for the most effective inhibitor. This was first demonstrated using the trypsin-like serine protease human urokinase. Urokinase (UK) has been shown to be strongly associated with tumor cells and to play a role in basement membrane degradation. Furthermore, inhibitors of the enzyme have been reported to slow tumor metastasis as well as the growth of the primary tumor. Thus, UK has been a target for potent inhibitors that could be of value in cancer therapy. One family of inhibitors developed recently at Abbott Laboratories is based on naphthamidine as the parent compound, and five members of the family are shown in Scheme 1.

Using crystals supplied by our collaborators at Abbott, we were able to obtain Raman spectra for all five inhibitors, bound individually to crystals of UK. For each complex, data are markedly superior to those obtained in solution (*19*). All difference spectra of the bound inhibitors contain bands from the naphthyl ring and amidine group, as well as other functional groups. The Raman modes could be reproduced by quantum chemical analysis, giving a firm interpretation or prediction of the experimentally observed bands. In particular, the calculations indicated that protonation of the amidine group gives rise to a marker band near 1525 cm^{-1}. All complexes show this marker band, demonstrating that the amidine is protonated (see Figure 3), information that could not be obtained directly from X-ray crystallographic analysis. In a screen-type experiment, a mixture containing

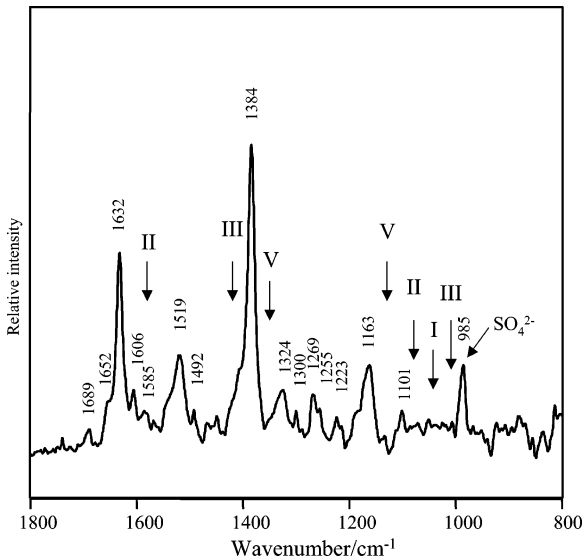

FIGURE 3: Results of a competitive inhibition experiment. Raman difference spectrum of inhibitor(s) bound to a UK crystal, derived from soaking in a mixture of five inhibitors.

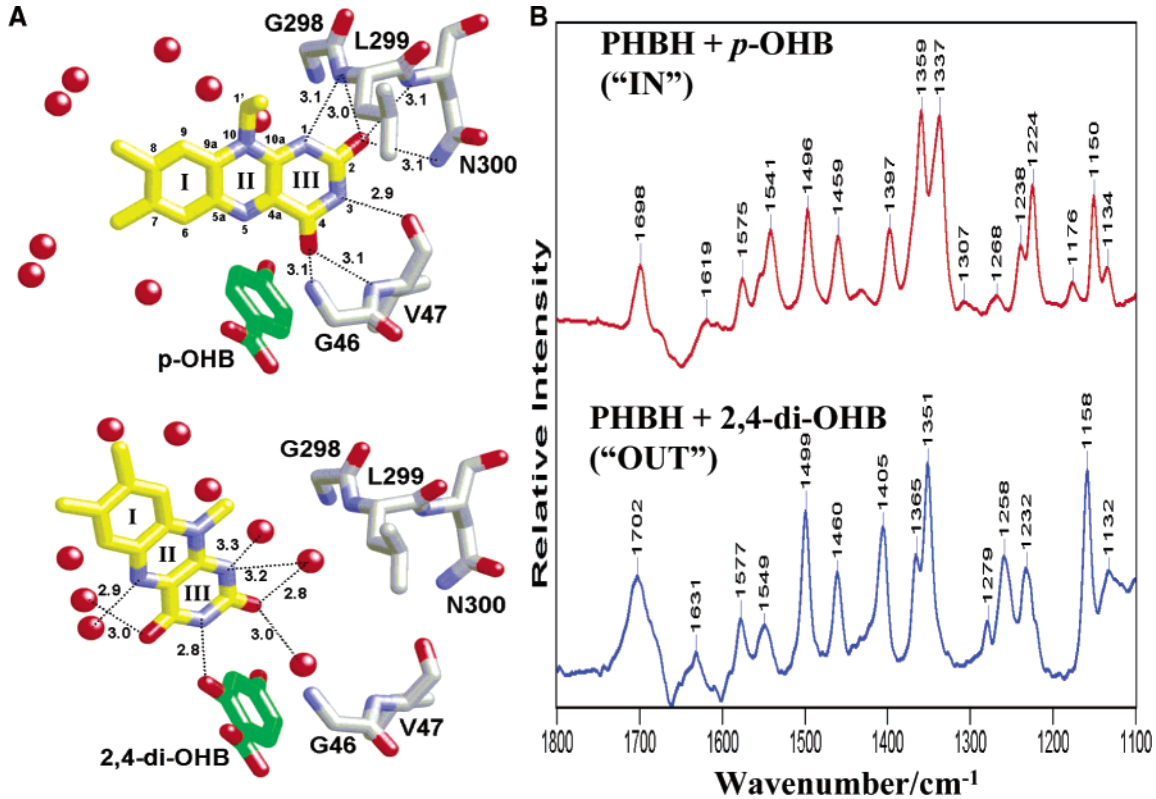

FIGURE 4: (A) Structures of the active sites of the PHBH complexes. Putative hydrogen bonds are depicted with dotted lines, and water molecules are shown as red spheres: (top) holo-PHBH with *p*-OHB (in conformation) and (bottom) holo-PHBH with 2,4-di-OHB (out conformation). Structures were obtained from the Protein Data Bank [PDB entries 1PBE and 1DOD for holo-PHBH with *p*-OHB (in) and holo-PHBH with 2,4-di-OHB (out), respectively]. (B) Raman difference spectra for FAD bound to a wild-type PHBH single crystal: (top) holo-PHBH with *p*-OHB (in) and (bottom) holo-PHBH with 2,4-di-OHB (out).

equimolar amounts of each of the five inhibitors was added to the mother liquor containing a single crystal, and the system was allowed to equilibrate fully before the crystal with bound ligands was transferred to fresh mother liquor and the Raman spectrum was recorded. The difference spectrum in Figure 3 contains almost exclusively features of compound **IV**, indicating that this is the most effective inhibitor in the group that was studied. Marker bands from the other inhibitors, whose peaks are expected at the arrow positions shown in Figure 3, are not detected. The finding that compound **IV** is the best inhibitor is consonant with the K_i values determined in solution. This result suggests that the active site in the crystal can be readily accessed via solvent channels. Figure 3 demonstrates that Raman crystallography can be used to screen for the most effective inhibitor, while the spectroscopic data do, at the same time, provide some insight into the chemistry of binding; in this case, the Raman spectra provide unique evidence of protonation of the amidine group.

Comparing Protein−Ligand Interactions in Crystals and in Solution

Since the dawn of macromolecular crystallography half a century ago, there have been arguments about how closely structures derived from single crystals resemble those found under more biologically relevant conditions, i.e., in solution. Using Raman crystallography, we can now ask if protein−ligand interactions vary between crystalline and solution complexes. The enzyme *p*-hydroxybenzoate hydroxylase (PHBH) makes an intriguing case study since its flavin cofactor migrates between two sites on the protein during the catalytic cycle (*20*). In one site, the "in" conformation (Figure 4), the flavin's isoalloxazine ring is essentially buried in a protein pocket. This form is present when the substrate 4-hydroxybenzoic acid (*p*-OHB) binds to PHBH. In contrast, when the substrate analogue 2,4-dihydroxybenzoic acid (2,4-diOHB) binds, the flavin ring is forced into the "out" conformation (Figure 4) where it is surrounded by water molecules. The Raman spectra for the isoalloxazine ring modes are compared for the in and out forms in Figure 4, and as can be seen, there are marked differences (*21*). Examination of the Raman marker bands for the in conformers in the solution and crystalline forms of the enzyme revealed that they are indistinguishable. However, there are small but significant differences in the positions of the out marker bands (*13*). These differences were ascribed to differences in the structure of the water molecules surrounding the flavin ring in solution and in the crystal. Another general difference between the flavin modes from PHBH in solution and single crystals is that crystallization results in a narrowing of the band profiles, by up to 30%. The narrowing is interpreted in terms of the protein being more restrained in its dynamical movements in the crystalline phase, and thus, the flavin ring exists in a more limited range of closely related conformational states in the crystal than in solution.

The relationship between Raman line widths and protein dynamics has been explored further for insulin molecules (*22*). Insulin, with a molecular mass of 5.8 kDa, normally exists as a hexamer, but mutant forms can result in the

appearance of entirely dimeric or monomeric species in solution. The amide I profile was taken as a measure of conformational heterogeneity, with line broadening attributed to a wider range of rapidly interconverting conformational states. The observation that the amide I profile narrowed progressively upon going from monomer to dimer to hexamer in solution and finally to hexamer in the crystalline phase was ascribed to the progressive mechanical damping of insulin chain fluctuations with an increase in the extent of insulin assembly.

Protein Conformational Changes in Single Crystals

When ligands soak into crystals and bind to active sites, there is often a change in protein conformation accompanying binding. This is usually reversible and may be localized around the active site or transmitted throughout larger segments of the protein. We will illustrate this using, again, the example of MM-CoA binding in crystals of the 12S subunit of transcarboxylase. In addition, during the course of hundreds of experiments on single crystals, we have found serendipitously that ligand binding, and other effects, can occasionally bring about catastrophic changes in protein conformation within the crystal when most or all of the secondary structure in the crystal is irreversibly converted to β-sheet.

Cooperative Conformational Change Induced by Binding of MM-CoA to 12S. Binding of MM-CoA to the active sites within a 12S crystal leads to a modest conformational change in the protein (*17*). As a consequence of the conformational change, the protein's Raman spectrum changes, and in the Raman difference spectrum ([protein + ligand] minus [protein]), the difference between the protein modes does not equal zero. In this kind of experiment, ligand modes always appear in the "positive" direction (above the baseline), while protein features usually appear in the positive and negative directions. This is seen clearly in the Raman difference spectrum in Figure 2B, where many features are assigned by Zheng et al. (*17*) to peptide group motions and to aromatic side chains (whose environments have been modified by MM-CoA binding). Most band assignments are accurate, being based on 30 years of knowledge available in the protein Raman literature and extensive recent studies in Raman crystallography. One limitation of the data on conformational change is that unless site-directed isotope editing is used (*23*) it is not possible to determine the region in which the protein conformational change is occurring. However, the intensity of the amide modes in the difference spectra allows us to estimate that the conformational change involves only a few percent of the total peptide linkages.

As discussed earlier, the adenine peak near 724 cm^{-1} can be used to quantitate the amount of bound MM-CoA and Figure 2B allows us to determine that there are six MM-CoAs per hexamer, resulting from a prolonged soaking-in experiment. Figure 2C shows from a soak-out experiment that only two molecules of MM-CoA per 12S hexamer are left. Although the ligand modes are greatly reduced in intensity, the protein bands in the difference spectrum are unchanged. This was an early indication that MM-CoA binding brings about a cooperative change in protein conformation. This has been confirmed by carefully titrating MM-CoA into crystals of 12S and, in separate experiments

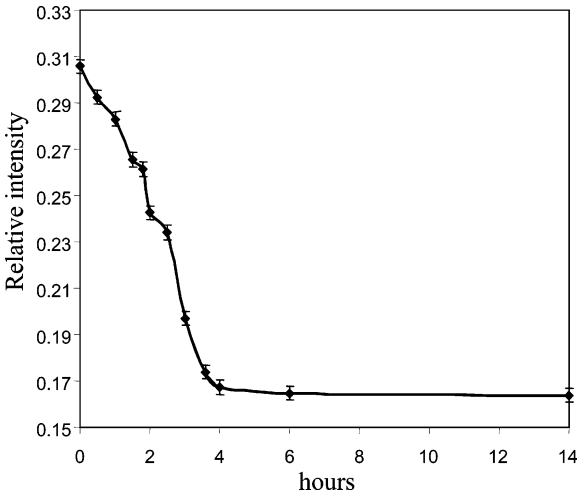

FIGURE 5: Time-dependent changes of Raman intensity at the helix marker band at 940 cm^{-1} from the 5S subunit of transcarboxylase after the pH is reduced from 6.5 to 4.5. The Raman intensity at 1450 cm^{-1} is used as a reference.

in solution, by isothermal calorimetry (unpublished results from this laboratory). A complete conformational change occurs upon binding one to two MM-CoAs per hexamer, and no further change is observed when the next four ligands bind in the hexamer. The cooperative conformational change is linked intimately with the labile COO^- group on the methylmalonyl group since binding of the product, propionyl-CoA (eq 1), does not bring about a conformational change. The availability of difference spectra (Figure 2B,C) allows us to subtract spectrum C from spectrum B, which eliminates the protein modes and leaves the spectrum of just bound MM-CoA without any contribution from the protein; this is seen in Figure 2D.

Massive Conformational Changes within Crystals. The precise positions of Raman amide I and III bands are distinctive for β-sheet and α-helical secondary structures, and in addition, α-helices show characteristic Raman intensities near 1340 and 940 cm^{-1}. Thus, it is trivial to identify these marker bands in single-crystal spectra. In 2000, Raman crystallographic studies commenced on transcarboxylase's other major subunit, the so-called 5S, a 120 kDa dimer that converts bound pyruvate to oxaloacetate using CO_2^- from carboxybiotin (*15*). We were puzzled by the observation that the secondary structure Raman markers appeared to be very different for 5S from crystal to crystal. This was so different from our experience with many other crystal samples that we ignored the problem for some time. However, the underlying cause of the apparent variation in secondary structure was subsequently identified. The crystals grown at pH 7.0 showed a clear mixture of β-sheet and α-helical secondary structure Raman markers. But when the pH in the surrounding mother liquor to was reduced 5.0, the intensity of the α-helical markers declined dramatically, while those due to β-sheet increased (*24*). Figure 5 shows the decrease in the intensity of the characteristic α-helical feature near 940 cm^{-1} over a period of 4 h. This effect is irreversible.

Subsequently, we were able to show similar effects for other proteins, but using very different sets of perturbants. Insulin is ~50% α-helical, but when the S−S linkages in the crystal are reduced to SH, all α-helical markers disappear from the Raman spectrum of the crystal and are replaced by

Scheme 2: Structure of β-Lactamase Inhibitors

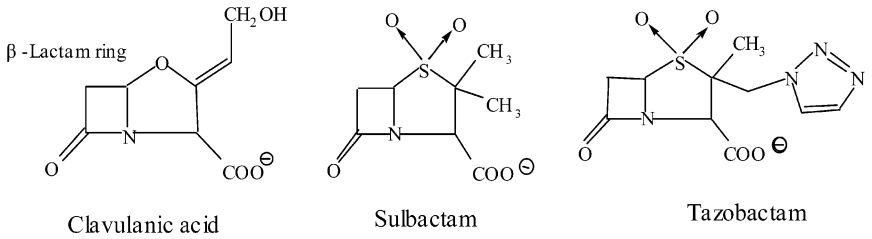

Clavulanic acid Sulbactam Tazobactam

β-sheet bands. The behavior of the 12S subunit is even more bizarre (*24*). 12S crystals do not appear to be sensitive to pH changes, and they undergo only small reversible conformational changes upon binding the substrate MM-CoA. However, when both substrates, MM-CoA and biotin, are added to the mother liquor around 12S crystals, the protein converts from a mixture of α-helix and β-sheet to entirely β-sheet.

Though we are far from understanding the mechanics of these wholesale conformational changes, all three proteins examined thus far, 12S, 5S, and insulin, share the same properties in their β-sheet-converted forms. (1) The change to predominantly β-sheet is irreversible. (2) The crystal morphology remains unchanged, but it no longer diffracts X-rays. (3) The crystal's solubility is greatly diminished. (4) The converted crystals can be stained with Congo red and thioflavin S, whereas the native crystals cannot.

These factors suggest that proteins in crystals can undergo relatively massive conformational changes to form β-sheet secondary structure and that intermolecular sheets are likely formed. The effect occurs only rarely and is catalyzed by widely divergent conditions, and it is difficult to characterize by any other means apart from Raman microscopy, mostly due to the loss of solubility and diffraction. The observed changes are not due to an increase in temperature caused by a laser beam; the temperature in the hanging drop increases by ~10 °C during irradiation, but the conformational changes occur only after addition of the appropriate chemical perturbant.

Reaction Intermediates in Crystals: β-Lactamases and Drug Resistance

Raman crystallography can identify and follow the populations of reaction intermediates in single crystals. For this to be effective, the reactions must occur on time scales of longer than 1 min. The time scale is set by the need to accumulate the Raman data for ≥1 min on the CCD detector. The other complication arises from possible population heterogeneity in the crystal caused during substrate soakins by the reaction occurring near the surface of the crystal prior to the substrate reaching the middle of the crystal. However, if these limitations do not apply, or can be overcome, the approach is very powerful.

At this time, the best developed example concerns β-lactamase enzymes reacting with three drugs that are used widely in the clinic (*25*, *26*). Penicillin and its analogues kill bacteria by interfering with cell wall synthesis. However, bacteria produce enzymes, β-lactamases, that hydrolyze penicillin before it can attack the bacterium. Therefore, it is standard clinical practice to prescribe a second drug with penicillin that will block the active site of the β-lactamase. However, in turn, bacteria produce mutated forms of β-lactamase that are not blocked by the inhibitor drug. This is a major source of drug resistance. A main goal of the Raman crystallographic analysis of β-lactamase−drug reactions is to compare the reactions involving wild-type and mutant enzymes and thus elucidate the molecular determinants of drug resistance.

The three commonly used β-lactamase inhibitors are shown in Scheme 2. They are known as suicide, or mechanism-based, inhibitors because they react chemically with the enzyme via a complex reaction pathway. Although the latter has been mapped out in some detail over the past 30 years, key questions remain unresolved. In the context of drug resistance, which species on the reaction pathway are most effective in inhibiting the enzyme, and do single-site mutations affect the structure or populations of intermediates, or both of these properties? These reactions can be studied by Raman crystallography because important intermediates are formed on the time scale of minutes to tens of minutes and because the substrates soak into the crystals in only ~1 min, minimizing the effect of kinetic heterogeneity within the inner and outer layers of the crystal. Initial studies utilized a single mutated form of the enzyme (E166A) that has a deacylation step on the pathway blocked by removal of E166. Thus, the intent is to focus initially on the acyl−enzyme species that exists in the reaction scheme (*18*).

Figure 6 compares the Raman spectrum of the free drug tazobactam with the Raman difference spectrum for tazobactam infusing into an E166A lactamase crystal for 2 min and for 28 min. The Raman difference spectra contain few modes that can be assigned to the parent tazobactam. A key observation is that there is no trace of the lactam C═O stretch near 1780 cm^{-1}, showing that lactam ring opening has occurred within the dead time of our experiment, essentially 2 min. A peak grows in with time at 1593 cm^{-1} (*18*); detailed analysis using NH−ND exchange and quantum mechanical calculations assigned this feature to a stretching vibration from the *trans*-enamine species (see Scheme 3). All three inhibitors exhibited a peak in this region, and we were able to use its intensity variation to follow population changes for the intermediates in the crystal. These are shown in Figure 7. Interestingly, tazobactam, the compound with the greatest clinical efficacy, has the highest build-up of the *trans*-enamine species.

Being able to follow population changes in crystals is of very great value for X-ray crystallographic studies. Prior to the Raman crystallographic analysis, crystallographers frequently flash-froze crystals to trap intermediates during soakin experiments. However, this was necessarily very much on a hit-and-miss basis. Now, however, Raman data can guide the conditions and time for flash-freezing. Figure 7 shows that the putative enamine population for tazobactam

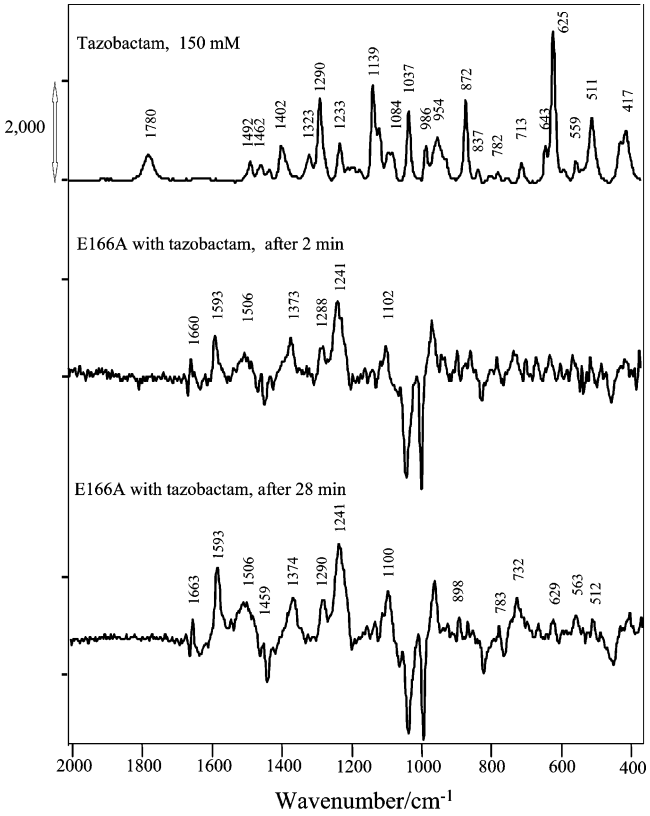

FIGURE 6: Raman difference spectra of free tazobactam (top trace) and tazobactam soaking into an E166A β-lactamase crystal at different times (middle and bottom traces). The vertical bar denotes a 2000-photon event.

Scheme 3: Two Possible Acyl−Enzyme Enamine Species in the E166A Lactamase Crystal

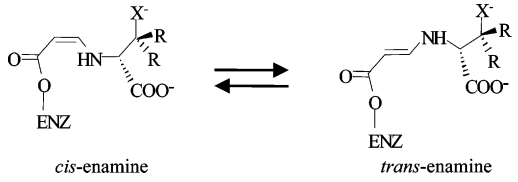

reaches a maximum at ~28 min. Using the 28 min soak time, our crystallographer colleagues were able to trap a stoichiometric tazobactam−β-lactamase complex with one *trans*-enamine per active site (*27*). A cartoon of the active site derived from this structure is shown in Scheme 4. The structure reveals favorable interactions involving tazobactam's SO_2 group and triazolyl rings. However, sulbactam lacks a triazolyl ring, and clavulanic acid lacks both the ring and an SO_2 group. This may in part explain why tazobactam is a superior inhibitor; it may form a more stable enamine and thus more effectively block the active site.

Future Possibilities and Limitations

The examples described above offer evidence that Raman crystallography may be applied to a wide range of systems. Although it can have a powerful synergy with X-ray crystallographic analysis, X-ray diffraction quality crystals are not needed, so for example, Raman difference data can be obtained from twinned crystals or microcrystalline powders. The difference Raman approach is most facile when ligands can be soaked in and soaked out of crystals. However, with careful attention to crystal alignment, Raman difference

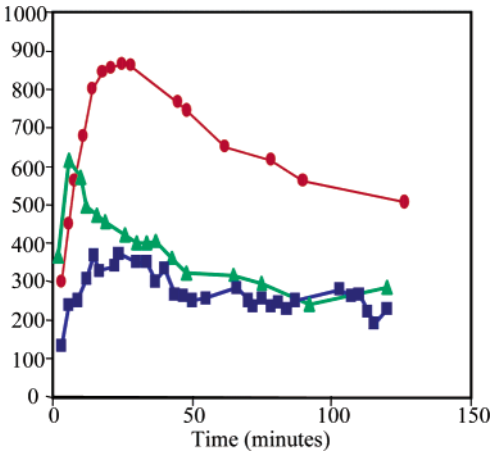

FIGURE 7: Time dependence of enamine peak height near 1593 cm^{-1} (normalized to the amide I band) for the E166A crystal and three inhibitors in H_2O: (red circles) tazobactam, (green triangles) sulbactam, and (blue squares) clavulanate.

Scheme 4: Diagram of Tazobactam Bound to the E166A Mutant of SHV-1 β-Lactamase[a]

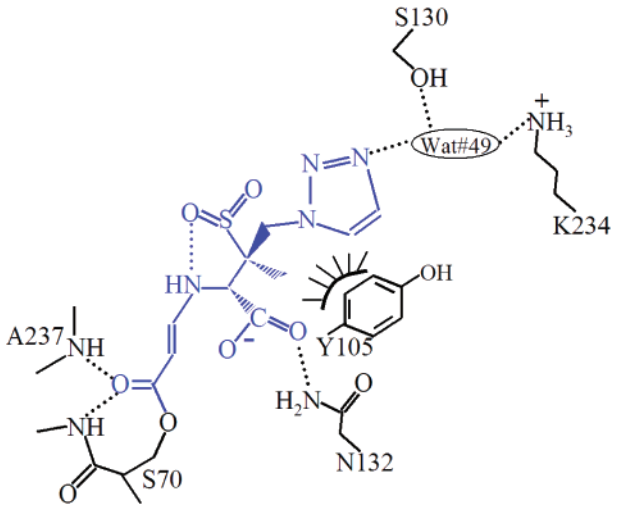

[a] Hydrogen bonds are highlighted as dotted lines, and the hydrophobic van der Waals interactions between Y105 and the triazolyl ring and methyl moieties of tazobactam are depicted with the hatched curved line.

data can be obtained from two crystals, one in the apo form and the other containing the ligand. The best data are collected from systems in which the target ligand is a strong Raman scatterer, and this usually means that the ligand has a delocalized π-electron chain. Thus, ligands lacking any conjugation, for example, carbohydrate-based compounds, present a greater challenge.

Our microscope system provides acceptable signal-to-noise ratio data with data accumulation for ~100 s. Technical improvements may reduce this by a factor of 10, but subsecond data accumulation, at least for nonresonance Raman spectra, is not on the immediate horizon. An imminent development in the field is Raman cryocrystallography. Flash-freezing crystals to extend the lifetime in the X-ray beam and to improve resolution is a routine procedure in X-ray crystallography. However, there is concern that flash-freezing may perturb the native room-temperature conformation, at least at the level of side chain conformations (*28*). Low-temperature Raman crystallography is well poised to address these concerns, and we have shown

recently that high-quality Raman spectra of lysozyme, with cryoprotectant, can be obtained in a cold nitrogen stream at 150 K (unpublished data from this laboratory).

ACKNOWLEDGMENT

It is a pleasure to express the great debt of gratitude we owe to our many colleagues and collaborators whose names are listed in our publications.

REFERENCES

1. Carey, P. R., and Tonge, P. J. (1995) Unlocking the secrets of enzyme power using Raman spectroscopy, *Acc. Chem. Res. 28*, 8−13.
2. Carey, P. R. (1999) Raman spectroscopy, the sleeping giant in structural biology, awakes, *J. Biol. Chem. 274*, 26625−26628.
3. Callender, R. H., and Deng, H. (1994) Nonresonance Raman difference spectroscopy: A general probe of protein structure, ligand binding, enzymatic catalysis, and the structures of other biomacromolecules, *Annu. Rev. Biophys. Biomol. Struct. 23*, 215−245.
4. Yu, N.-T. (1974) Comparison of protein structure in crystals, in lyophilized state, and in solution by laser Raman scattering. 3. α-Lactalbumin, *J. Am. Chem. Soc. 96*, 4664−4668.
5. Zhu, L., Sage, J. T., and Champion, P. M. (1993) Quantitative structural comparisons of heme protein crystals and solutions using resonance Raman spectroscopy, *Biochemistry 32*, 11181−11185.
6. Morikis, D., Sage, J. T., Rizos, A. K., and Champion, P. M. (1988) Resonance Raman studies of myoglobin single-crystals, *J. Am. Chem. Soc. 110*, 6341−6342.
7. Loppnow, G., Barry, B., and Mathies, R. (1989) Why are blue visual pigments blue? A resonance Raman microprobe study, *Proc. Natl. Acad. Sci. U.S.A. 86*, 1515−1518.
8. Puppels, G. J., de Mul, F. F., Otto, C., Greve, J., Robert-Nicoud, M., Arndt-Jovin, D. J., and Jovin, T. M. (1990) Studying single living cells and chromosomes by confocal Raman microspectroscopy, *Nature 347*, 301−303.
9. Smulevich, G., and Spiro, T. G (1993) Single-crystal micro-Raman spectroscopy, *Methods Enzymol. 226*, 397−408.
10. Li, T., Chen, Z., Johnson, J. E., and Thomas, G. J., Jr. (1992) Conformations, interactions, and thermostabilities of RNA and proteins in bean pod mottle virus: investigation of solution and crystal structures by laser Raman spectroscopy, *Biochemistry 31*, 6673−6682.
11. Benevides, J. M., Terwilliger, T. C., Vohnik, S., and Thomas, G. J., Jr. (1996) Raman spectroscopy of the Ff gene V protein and complexes with poly(dA): nonspecific DNA recognition and binding, *Biochemistry 35*, 9603−9609.
12. Thomas, G. A., Kubasek, W. L., Peticolas, W. L., Greene, P., Grable, J., and Rosenberg, J. M. (1989) Environmentally induced conformational changes in B-type DNA: comparison of the conformation of the oligonucleotide d(TCGCGAATTCGCG) in solution and in its crystalline complex with the restriction nuclease EcoRI, *Biochemistry 28*, 2001−2009.
13. Altose, M. D., Zheng, Y., Dong, J., Palfey, B. A., and Carey, P. R. (2001) Comparing protein−ligand interactions in solution and single crystals by Raman spectroscopy, *Proc. Natl. Acad. Sci. U.S.A. 98*, 3006−3011.
14. Tsuboi, M., and Thomas, G. J., Jr. (1997) Raman scattering tensors in biological molecules and their assemblies, *Appl. Spectrosc. Rev. 32*, 263−299.
15. Wood, H. G., and Zwolinski, G. (1976) Transcarboxylase: role of biotin, metals, and subunits in the reaction and its quaternary structure, *CRC Crit. Rev. Biochem. 4*, 47−122.
16. Hall, P. R., Wang, Y. F., Rivera-Hainaj, R. E., Zheng, X. J., Pusztai-Carey, M., Carey, P. R., and Yee, V. C. (2003) Transcarboxylase 12S crystal structure: hexamer assembly and substrate binding to a multienzyme core, *EMBO J. 22*, 2334−2347.
17. Zheng, X., Rivera-Hainaj, R. E., Zheng, Y., Pusztai-Carey, M., Hall, P. R., Yee, V. C., and Carey, P. R. (2002) Substrate binding induces a cooperative conformational change in the 12S subunit of transcarboxylase: Raman crystallographic evidence, *Biochemistry 41*, 10741−10746.
18. Helfand, M. S., Totir, M. A., Carey, M.-P., Hujer, A. M., Bonomo, R. A., and Carey, P. R. (2003) Following the reactions of mechanism-based inhibitors with β-lactamase by Raman crystallography, *Biochemistry 42*, 13386−13392.
19. Dong, J., Swift, K., Matayoshi, E., Nienaber, V. L., Weitzberg, M., Rockway, T., and Carey, P. R. (2001) Probing inhibitors binding to human urokinase crystals by Raman microscopy: Implications for compound screening, *Biochemistry 40*, 9751−9757.
20. Palfey, B., and Massey, V. (1998) Flavin-dependent enzymes, in *Comprehensive Biological Catalysis, A Mechanistic Reference* (Sinnott, M., Ed.) Radical Reactions and Oxidation/Reduction, Vol. 3, pp 83−154, Academic Press, San Diego.
21. Zheng, Y. G., Dong, J., Palfey, B. A., and Carey, P. R. (1999) Using Raman spectroscopy to monitor the solvent-exposed and "buried" forms of flavin in p-hydroxybenzoate hydroxylase, *Biochemistry 38*, 16727−16732.
22. Dong, J., Wan, Z. L., Popov, M., Carey, P. R., and Weiss, M. A. (2003) Insulin assembly damps conformational fluctuations: Raman analysis of amide I linewidths in native states and fibrils, *J. Mol. Biol. 330*, 431−442.
23. Dong, J., Wan, Z., Chu, Y., Nakagawa, S., Katsoyannis, P., Weiss, M. A., and Carey, P. R. (2001) Isotope-edited Raman spectroscopy of proteins: A general strategy to probe individual peptide bonds with application to insulin, *J. Am. Chem. Soc. 123*, 7919−7920.
24. Zheng, R., Zheng, X., Dong, J., and Carey, P. R. (2004) Proteins can convert to β-sheet in single crystals, *Protein Sci. 13*, 1288−1294.
25. Helfand, M. S., and Bonomo, R. A. (2003) β-Lactamases: a survey of protein diversity, *Curr. Drug Targets: Infect. Disord. 3*, 9−23.
26. Page, M. G. (2000) β-Lactamase inhibitors, *Drug Resist. Updates 3*, 109−125.
27. Padayatti, P. S., Helfand, M. S., Totir, M. A., Carey, M. P., Hujer, A. M., Carey, P. R., Bonomo, R. A., and van den Akker, F. (2004) Tazobactam forms a stoichiometric trans-enamine intermediate in the E166A variant of SHV-1 β-lactamase: 1.63 Å crystal structure, *Biochemistry 43*, 843−848.
28. Halle, B. (2004) Biomolecular cryocrystallography: Structural changes during flash-cooling, *Proc. Natl. Acad. Sci. U.S.A. 101*, 4793−4798.

BI049138A